14th International Symposium on Turbulence and Shear Flow Phenomena (TSFP14)
Heidelberg, Germany, July 28–31, 2026

EFFECT OF BOUNDARY LAYER DEVELOPMENT ON FLOW SEPARATION OVER THE BEVERLI HILL

Nicole-Marie Sa'adeh, Daniel MacGregor, and Philippe Lavoie
Institute for Aerospace Studies
University of Toronto
4925 Dufferin St., Toronto, ON, M3H 5T6, Canada
nicole.saadeh@mail.utoronto.ca, daniel.macgregor@mail.utoronto.ca,
phil.lavoie@.utoronto.ca

ABSTRACT

An experimental study on flow separation over a three-dimensional hill at three Reynolds numbers was conducted at the University of Toronto Institute for Aerospace Studies (UTIAS). Mean surface pressure measurements point to weak separation for the lowest Reynolds number. Assessment of the relaminarization parameter reveal a high propensity of the low Reynolds number to relaminarize. Furthermore, normalized velocity fluctuations obtained from Particle Image Velocimetry reveal high magnitudes at this low Reynolds number, with large fluctuations in the local frame, indicating retranstion. A Lagarangian approach was used to identify the mean separation point along the centreline of the model and revealed further Reynolds number dependency, where the lower Reynolds number separates farther downstream than the higher two Reynolds numbers tested. This is attributed to the re-energized inner layer due to partial retransition in the leeward adverse pressure gradient region of the model.

INTRODUCTION

In many engineering flows of interest, turbulent boundary layers (TBLs) are three-dimensional (3D) and experience both streamwise and spanwise pressure gradients. These spanwise pressure gradients result in spanwise shear, therefore skewing the boundary layer (Devenport & Lowe, 2022). This poses a challenge as there is no universally accepted mean velocity profile equation describing skewed 3D TBLs (Duetsch-Patel *et al.*, 2023). Additionally, many commercially used turbulence models employed in Reynolds-Averaged Navier-Stokes (RANS) CFD rely on theories developed for two-dimensional boundary layers, thus limiting the accuracy of RANS with 3D flows, as well as flows with large separation (Gargiulo *et al.*, 2021). A crucial step for improved turbulence modelling capabilities is validating CFD against high quality experimental data. The Benchmark Validation Experiments for RANS and LES (Large Eddy Simulation) Investigations (BeVERLI) is a 3D bump model developed as part of an ongoing international effort motivated by NATO's Applied Vehicle Technology Panel (AVT-413), titled *Physics and Modeling of Separated Flows Around Smoothly-Curved Bodies*. The panel's focus is on improving the understanding of the fundamental physics of three-dimensional incompressible Reynolds number flow separation around smoothly curved bodies.

Experimental studies on hill geometries have been conducted in the past including a Gaussian-shaped bump called the Boeing bump by Gray *et al.* (2023). The Direct Numerical Simulation (DNS) studies of Balin & Jansen (2021) and Uzun & Malik (2021) with the Boeing bump revealed interesting flow phenomena, namely relaminarization and retransition, in their low Reynolds number case. In a strong favourable pressure gradient (FPG), the flow can accelerate enough to undergo relaminarization. When this happens, the TBL develops a viscous dominated inner layer and the Reynolds stresses and turbulent kinetic energy (TKE) drop significantly when scaled with inner variables (friction velocity, u_τ) (Balin & Jansen, 2021). Additionally, in strong FPG and adverse pressure gradient (APG) regions, the inner and outer layers de-couple, becoming largely independent of each other. The inner layer is dominated by pressure gradient effects, and the outer layer, behaving more like a free-shear layer, responds to pressure gradient and streamline curvature effects (Balin & Jansen, 2021; Uzun & Malik, 2021). In the subsequent APG region past the apex of the Boeing bump, the partially relaminarized flow experiences instabilities strong enough to transition back to a turbulent state. A large spike is observed in the wall-normal TKE and Reynolds shear stress in the downstream APG, and this re-energized inner layer is able to resist the leeward APG region, leading to incipient or weak separation. This results in delayed flow separation at low Reynolds numbers, counter to expectations.

On the BeVERLI hill, Virginia Tech noticed relaminarization via an upstream separation bubble from their surface oil flow visualization for the 0° orientation at a bump height Reynolds number of Re_h = 114k (Gargiulo *et al.*, 2021; Williams *et al.*, 2022). Beyond this Reynolds number, the upstream separation bubble washes away.

This paper explores relaminarization and retransition for the 45° orientation of the BeVERLI hill. At the 45° orientation, VT compared the experimental and RANS mean pressure coefficient along the hill centreline. They found that both RANS methods used failed to predict the separation downstream of the hill apex, and more interestingly, the RANS methods were deficient in predicting the complex physics found in the flat-top region of the hill where the flow at the Reynolds numbers tested was still attached (Gargiulo *et al.*, 2023). Discrepancies were more pronounced for the lowest Reynolds number, indicating that the physical characteristics of the flow are Reynolds number dependent (Gargiulo *et al.*, 2023).

The results shared here present evidence of relaminarization and retransition at the lowest Reynolds number tested with the BeVERLI hill along its centreline for the 45° orientation. Together, pressure measurements, velocity field statistics, and calculated parameters from their post-processing support this observation. Additionally, trends at higher Reynolds numbers facilitate meaningful comparison. These findings contribute to the expanding knowledge of 3D TBLs on smooth curved bodies and provide invaluable insight for the challenging tasks involved in the validation and improvement CFD turbulence modelling.

EXPERIMENTAL SETUP

The BeVERLI hill was developed by NASA and Virginia Tech and is characterized by a fifth-degree profile across its centreline, featuring 90° rotational symmetry, and consists of super-elliptic corners. Its detailed geometry is outlined by Gargiulo *et al.* (2020). A schematic of the bump geometry is shown in Figure 1a. The BeVERLI hill differs from other bump models in that it features a flat-top region, marked in red in Figure 1a, which introduces an additional adverse to favorable pressure gradient transition.

The recirculating wind tunnel at UTIAS was used for all experiments. The version of the hill used at UTIAS has a width, w, of 0.6 m and a height, h, of 0.12 m. A schematic of the experimental setup is shown in Figure 1b. The BeVERLI hill is made of 6061 aluminum and anodized in a matte black finish. The global coordinate system, seen in red in Figure 1b, is defined at the bump centre, co-planar with the flat-plate setup that the bump sits on. The bump orientation of interest is the 45° orientation, defined as when the fifth-degree polynomial that describes the hill is at a 45° angle to the incoming airflow, such that the free-stream velocity, U_∞, approaches the hill at one of its four corners, as seen in Figure 1b. The Reynolds number is based on the hill height, and experiments were conducted for Re_h = 38k - 208k.

Mean static pressure measurements on the BeVERLI hill were acquired using 135 surface pressure taps. The pressure ports have a diameter of 1/16 inch, and are connected to flexible Tygon tubing via small steel tubes. The pressure array consists of 40 ± 2 kPa differential pressure transducers. A pitot-static tube placed about 1.5 m upstream of the hill was used to measure the free-stream velocity. The pitot-static tube was connected to an MKS 225AD Baratron differential pressure transducer.

Two-component Particle Image Velocimetry (PIV) measurements obtained at six fields of view (FOVs) in the $x-y$ plane along the hill centreline, encompassing roughly $-4h$ to $6h$ with respect to the global origin. For each of the six FOVs, two sCMOS LaVision cameras were used side-by-side, stitching together both views to produce a single FOV. The tunnel was seeded with Sigma-Aldrich Bis(2-ethylhexyl) sebacate to give 1 μm diameter particles. A Quantel Evergreen 200 mJ Nd:YAG dual pulse laser was used, with a laser wavelength of 532 nm. A total of 2000 snapshots were obtained for each FOV at a frequency of 3 Hz for Re_h = 123k and 208k, and 2.5 Hz for Re_h = 38k. Subsequent data processing was carried out with DaVis 11 software and further processing was done in MATLAB.

RESULTS

Mean Surface Pressure

The contours of the mean surface pressure coefficient, C_p, are shown in Figures 2a-2c, and C_p distributions along the centreline are presented in Figure 2d. The flow encounters a strong APG at the upstream tip of the hill followed by an increasingly favourable pressure gradient. Then the flow encounters the switch from APG to FPG at the flat-top region, and finally the leeward APG region downstream. There are a few differences to note between the lowest Reynolds number, Re_h = 38k, and the others. First, the suction peaks along the sides of the centrespan are noticeably weaker at Re_h = 38k, noticeable in Figures 2a-2c. The leeward APG region is also less pronounced at Re_h = 38k. This is further reflected in the centreline C_p profile, where the slope of C_p (beginning at $x/h \approx 1.0$) is more shallow, indicating weak separation. Another difference appears upstream in the region $-0.56 < x/h < 0$, where the C_p values are higher at Re_h = 38k than for the higher Reynolds numbers, indicating that the flow here is more affected by the flat-top APG.

The propensity of a flow to relaminarize can be assessed with the relaminarization parameter, K, given by

$$K = \frac{\nu}{U_e^{*2}} \frac{\partial U_e^*}{\partial s}, \tag{1}$$

where U_e^* is the wall-parallel boundary-layer edge velocity, ν is the kinematic viscosity, and s is the surface distance. A value of K above 3×10^{-6} indicates the onset of relaminarization (Narayanan & Ramjee, 1969; Narasimha & Sreenivasan, 1973; Balin & Jansen, 2021; Gargiulo *et al.*, 2021). The wall-parallel boundary-layer edge velocity from Equation 1 was obtained by using the pressure coefficient and Bernoulli equation to give $U_e^* = \sqrt{1-C_p} \cdot U_\infty$. Along the centreline of the hill, K is plotted in Figure 2e. At Re_h = 38k, the flow exhibits a large propensity to relaminarize in the upstream FPG region, having exceeded the critical threshold, marked in the black dashed line, reaching a peak value of about 2×10^{-5}. Conversely, the value of K is significantly lower for the higher Re_h cases indicating that they are much less likely to relaminarize. The Re_h = 123k case crosses the threshold in a narrow region of the FPG, while the highest Reynolds number case does not reach the threshold.

Velocity Field

The mean Reynolds shear stress, $-\overline{u'v'}$, and turbulent kinetic energy, k, normalized with U_∞^2 are shown in Figure 3 for Re_h = 38k, 123k, and 208k. The different values in the contour plots of these fluctuations in the wake region indicate Reynolds number dependency, and, more interestingly, these values are highest for the lowest Reynolds number case.

To further assess this, local quantities along lines normal to the bump surface were obtained. Quantities taken along directions normal to the surface are denoted with a *. The boundary-layer thickness, δ_{99}, over the centreline of the BeVERLI hill was used to normalize the wall-normal distance, y^*. The diagnostic plot method of Vinuesa *et al.* (2016) was used to determine δ_{99}. It works by finding the location of y^* where the local turbulence intensity divided by the root of the shape factor, $u^*_{rms}/(\overline{U}^*\sqrt{H})$, is equal to 0.02, which correlates to $\overline{U}^*/U_e^*$ equaling 0.99, thereby obtaining both boundary-layer edge velocity and boundary-layer thickness. This is an iterative method where the initial guess for U_e^* is taken as the maximum of $\overline{U}^*$ at the line normal to the bump surface.

The local normalized TKE and Reynolds shear stress versus y^*/δ_{99} in the leeward APG region are plotted in Figure 4 and 5, respectively. As can be seen, there are large spikes of k^*/U_∞^2 and $-\overline{u'^*v'^*}/U_\infty^2$ at Re_h = 38k in the region of $y^*/\delta_{99} < 0.25$. These observations support the argument of retransition,

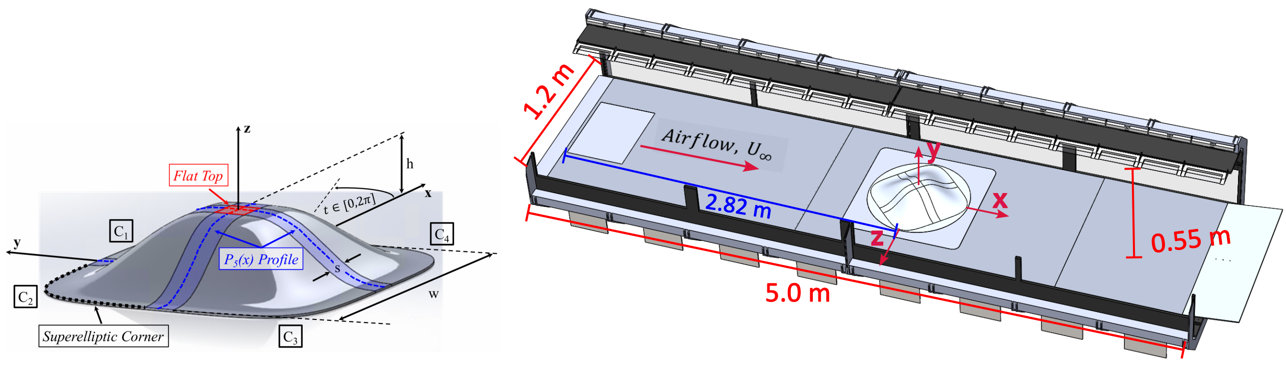

(a) (b)

Figure 1: a) Features of the BeVERLI Hill bump design from Gargiulo *et al.* (2020), b) Schematic of experimental setup

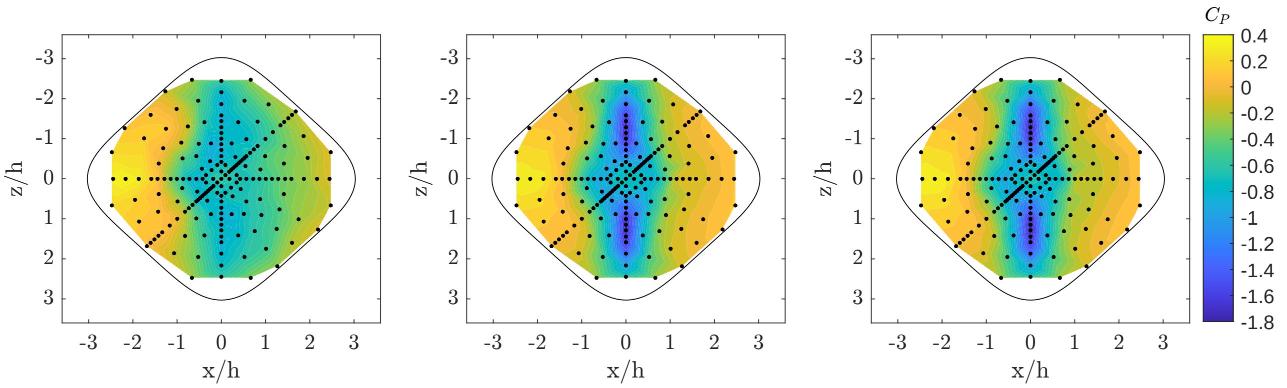

(a) Re_h = 38k (b) Re_h = 123k (c) Re_h = 208k

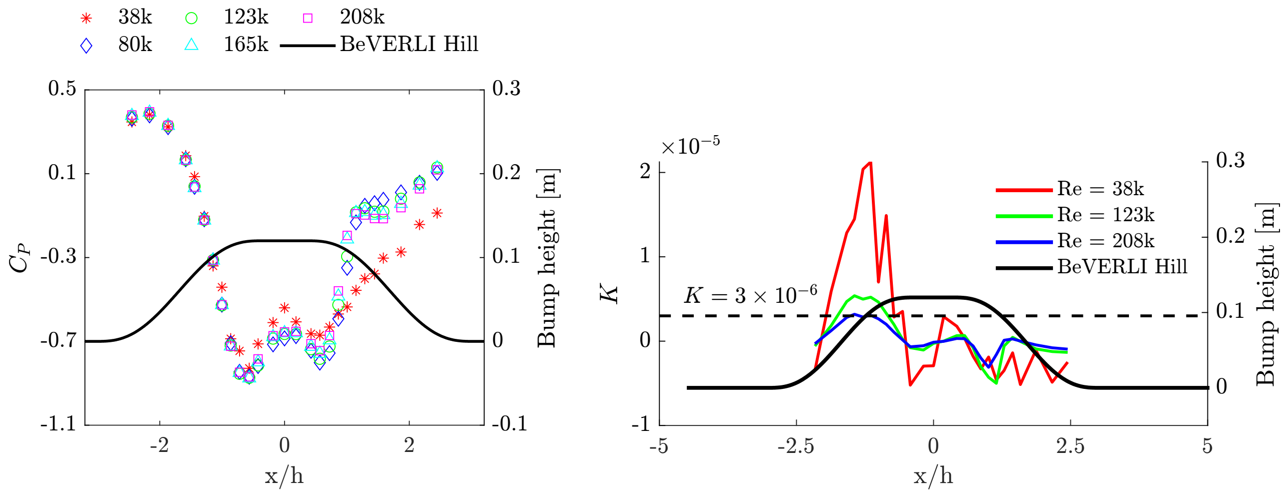

(d) Centreline C_p (e) Centreline K

Figure 2: Interpolated static pressure contours at Re_h = a) 38k, b) 123k, c) 208k; d) C_p along the centerline; e) Relaminarization parameter, K, along the hill centreline. U_∞ is approaching from left to right.

also observed by Balin & Jansen (2021) and Uzun & Malik (2021) with the Boeing bump, where the strong downstream APG region results in a large increases in the inner layer of these fluctuations at the low Reynolds number. Higher magnitudes of these values indicate a greater degree of turbulent mixing. The effects of retransition on the separation point of the flow are discussed in a later section.

Mean Shear Layer Dynamics

To assess the flow dynamics in the wake, Proper Orthogonal Decomposition (POD) was applied to the PIV data within a region spanning approximately 0.5h to 3h (PIV FOV 4), encompassing the separated flow. The first 10 POD modes of PIV FOV 4 correspond to 60% of the total energy for Re_h = 38k, 55% for Re_h = 123k, and 51% for Re_h = 208k, as seen in Figure 6a.

The reconstructed instantaneous streamwise velocity from the first 10 POD modes, denoted as $\tilde{U}$, was used to find

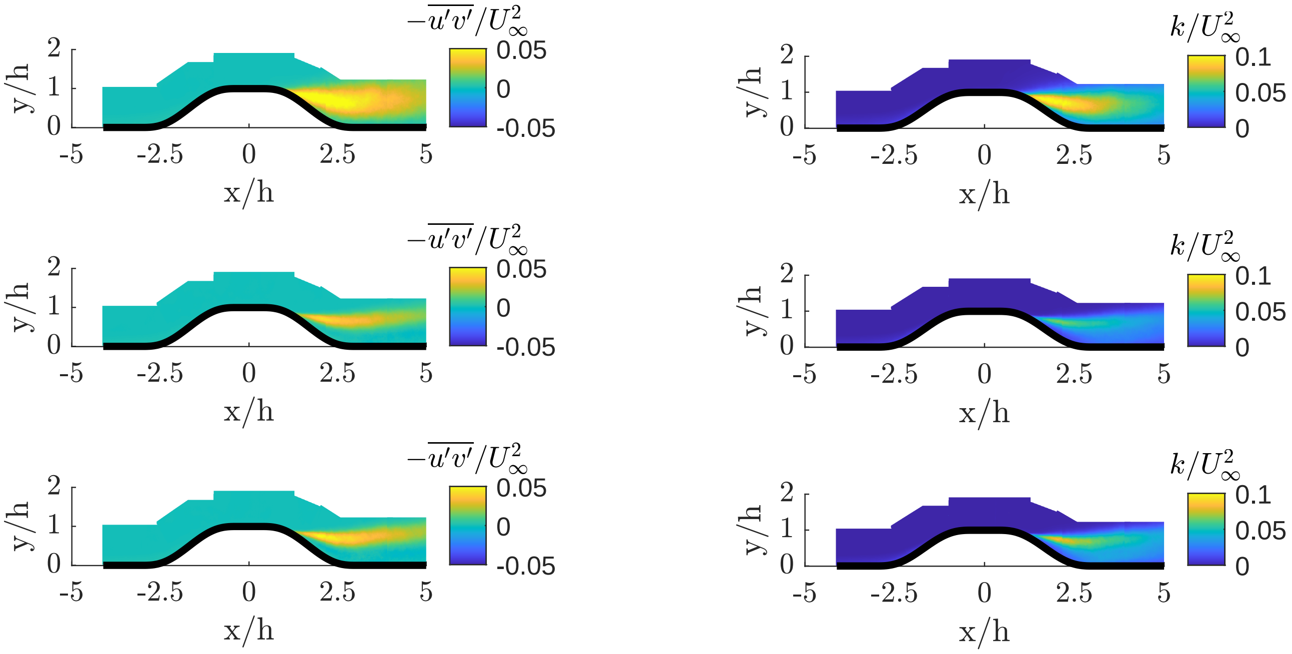

Figure 3: Mean Reynolds shear stress, $-\overline{u'v'}$, and turbulent kinetic energy, k, normalized with U_∞^2, along the hill centreline. Re_h = 38k (top), 123k (centre), and, 208k (bottom)

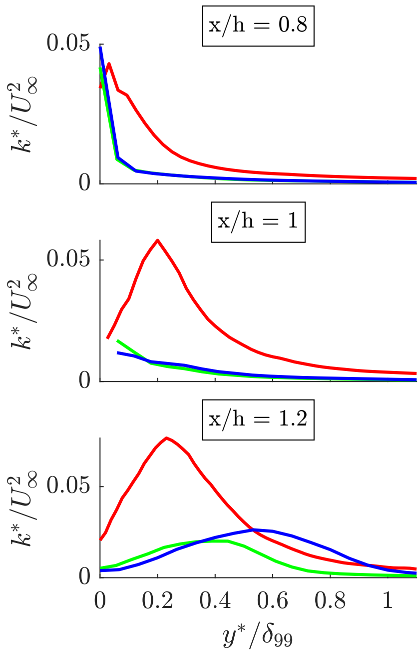

Figure 4: Local turbulent kinetic energy normalized with free-stream velocity, k^*/U_∞^2, along normal lines at $x/h =$ 0.8, 1.0, and 1.2. Re_h = 38k (red), 123k (green), and, 208k (blue)

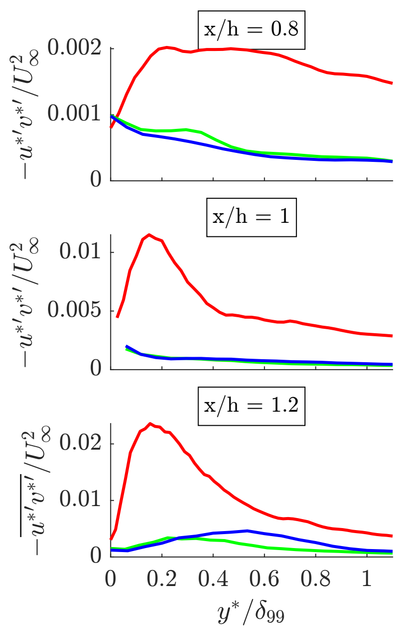

Figure 5: Local Reynolds shear stress normalized with free-stream velocity, $-\overline{u'^*v'^*}/U_\infty^2$, along normal lines at x/h = 0.8, 1.0, and 1.2. Re_h = 38k (red), 123k (green), and, 208k (blue)

the mean shear layer line at each snapshot. The global y coordinate of the mean shear layer line for each x location is defined as the location where $\tilde{U}/U_e = 0.5$. Here, U_e is taken as $0.99U_\infty$. The extent of the mean shear layer flapping is seen in Figures 6b and 6c, where 38 random snapshots at Re_h = 38k and 208k are plotted. The recirculating region at Re_h = 38k contracts and expands, resulting in a large flapping motion. In contrast, the recirculating region remains relatively consistent in size at Re_h = 208k, resulting in more localized, mild flapping of the shear layer. Though not shown here, the flapping motion at Re_h = 123k is similar to that of Re_h = 208k. The large flapping motion at Re_h = 38k, and the presumed de-coupling of the inner and outer layers in the upstream FPG region, allow the outer layer to engage earlier in turbulent mixing downstream, resulting in the high magnitudes of velocity fluctuations seen in the PIV data in Figure 3.

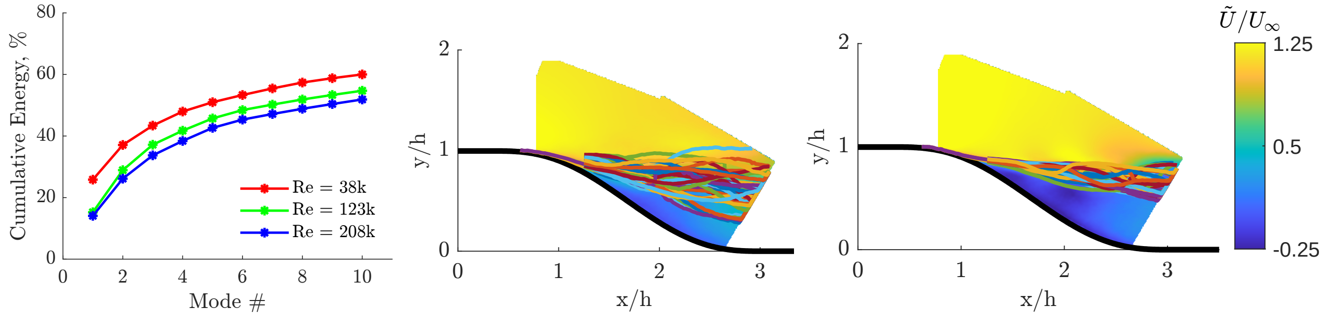

(a) POD Modes (b) Re_h = 38k (c) Re_h = 208k

Figure 6: a) Cumulative energy of the first 10 POD modes of PIV FOV 4. Mean shear layer lines from 38 snapshots overlaid on top of the reconstructed streamwise velocity from POD at a random snapshot normalized with free-stream velocity, $\tilde{U}/U_\infty$, at b) Re_h = 38k, and c) Re_h = 208k.

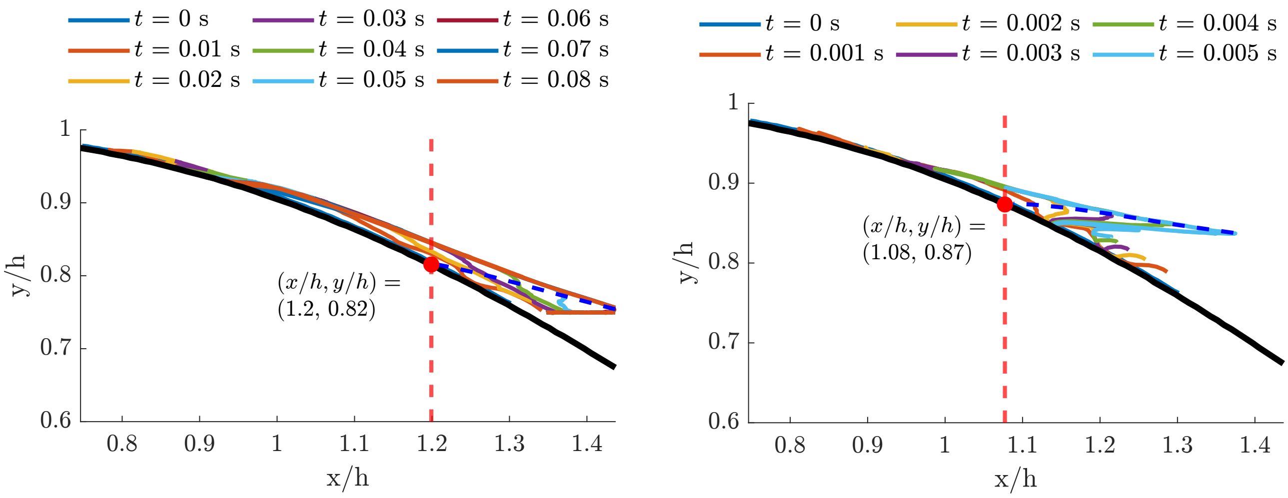

(a) $Re_h = 38k$ (b) $Re_h = 208k$

Figure 7: Material line trajectories and Lagrangian separation points at a) Re_h = 38k and b) Re_h = 208k

Lagrangian Separation

Identifying the mean separation point remains a topic of discussion among fluid dynamicists and modellers. Haller (2004) describes separation as the convergence and subsequent ejection of fluid from the vicinity of the boundary, attributing this to a "material spike". Emulating a procedure inspired by Serra *et al.* (2018, 2020), the mean separation point in the Lagrangian point of view was computed along the hill centreline using material spike trajectory by employing the mean velocity field data obtained from PIV. First, a finely spaced grid in the y-direction was defined where the first point is at the bump surface, and the y-value increases incrementally by dy = 0.1mm, so that material lines initially parallel to the wall can be generated. Mean streamwise and vertical velocities from PIV, $\overline{U}$ and $\overline{V}$, were linearly interpolated in y at this new finer grid using MATLAB's *interp2* function. Then, using a time step of dt = 0.001 s and a 4$^{\text{th}}$ order Runge-Kutta scheme, the intial coordinates of the fine grid, X_0 and Y_0, were translated in time using the interpolated mean velocities from an initial time t_0 = 0 s to a final time t_f = 3 s. The new positions of these points were calculated at each time step.

The spike formations of a material line initially parallel to the wall and 0.5 mm above the surface at Re_h = 38k and 208k are shown in Figures 7a and 7b, respectively. The blue dashed line is the backbone of the separation spike that was generated by connecting the curve maxima of the material line at each plotted time. This was then extrapolated to the wall, and the Lagrangian separation point is marked in red, where the separation spike backbone intersects the bump surface. The separation point for Re_h = 38k occurs farther downstream, at x/h = 1.2, compared to the higher Reynolds number, which exhibits separation at approximately $x/h \approx$ 1.1. The 123k Reynolds number, not shown here for brevity, also separates at $x/h \approx$ 1.1.

Plotted on Figure 8 are the Lagrangian and Prandtl separation points for all three Reynolds numbers. The Prandtl separation point is defined where the wall-shear stress, τ_w, is zero, and its longitudinal derivative, $\partial\tau_w/\partial x$ is negative. The Prandtl separation point is identified by the point at which the streamwise velocity first becomes negative. A summary of their coordinates is provided in Table 1. With both definitions of separation, the 38k Reynolds number is shown to consistently separate downstream of the higher two Reynolds numbers, and additionally, at all three Reynolds numbers, the Lagrangian separation points are upstream of the Prandtl separation points, consistent with the findings of the examples given by Serra *et al.* (2018, 2020).

As discussed in the preceding sections, the flow at Re_h = 38k displays large peaks of local fluctuation quantities, providing clues of retransition in the leeward APG region. This re-energized inner layer is able to resist the APG, leading to delayed separation downstream of the higher two Reynolds numbers, where the APG is weaker. Moreover, this separation is weak, as evidenced by the shallow slope of the centreline C_p in Figure 2d for $Re_h = 38$k.

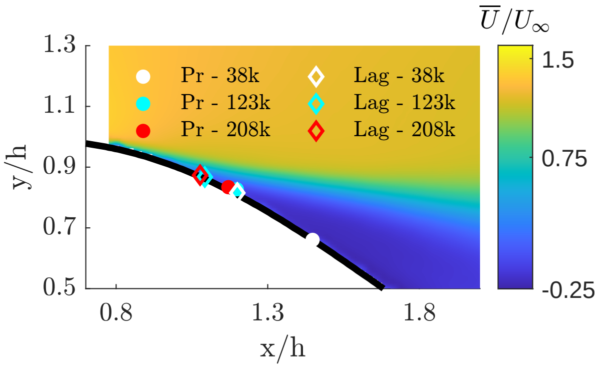

Figure 8: Lagrangian (diamond) and Prandtl (circle) points of separation at Re_h = 38k (white), 123k (cyan), 208k (red). Plotted on normalized streamwise velocity, $\overline{U}/U_\infty$ at Re_h = 208k.

Table 1: Coordinates of Lagrangian and Prandtl separation points

Re_h	Lagrangian point $(x/h, y/h)$	Prandtl point $(x/h, y/h)$
38k	(1.2, 0.82)	(1.45, 0.66)
123k	(1.1, 0.86)	(1.2, 0.83)
208k	(1.08, 0.87)	(1.17, 0.834)

CONCLUSIONS

To summarize the findings above, it is clear that the flow over the BeVERLI hill is complex and displays Reynolds number dependent trends for the range of conditions considered. The lowest Reynolds number has a greater propensity to relaminarize in the strong upstream FPG region. This is marked by the relaminarization parameter, K, and the noticeably higher C_p values in the flat-top APG, presumably due to the weakened turbulence from the upstream relaminarization. Additionally, a de-coupling between the inner and outer layers is postulated in the strong FPG region. Here, the outer layer behaves more like a free-shear layer, enabling earlier onset of turbulent mixing. This leads to increased normalized velocity fluctuations in the wake, as observed in the PIV results.

However, at Re_h = 38k the flow does not fully relaminarize, as residual instabilities in the inner layer remain sufficiently energetic to trigger retransition in the downstream APG region. Evidence of this retransition is seen as the weak separation by the shallow downstream slope in the centreline C_p profile, and is further supported by large peaks in k^* and $-\overline{u^{*\prime}v^{*\prime}}$ closer to the near-wall observed in the local reference frame at the lowest Reynolds number. Retransition at this Reynolds number results in delayed flow separation, with the Lagrangian and Prandtl mean separation points occurring downstream relative to those at higher Reynolds numbers along the hill centreline.

This flow behavior is consistent with phenomena observed in the Boeing bump, as reported in the DNS studies of Balin & Jansen (2021) and Uzun & Malik (2021).

REFERENCES

Balin, R. & Jansen, K. E. 2021 Direct numerical simulation of a turbulent boundary layer over a bump with strong pressure gradients. *Journal of Fluid Mechanics* **918**, A14.

Devenport, W. J. & Lowe, K. T. 2022 Equilibrium and non-equilibrium turbulent boundary layers. *Progress in Aerospace Sciences* **131**, 100807.

Duetsch-Patel, J. E., Gargiulo, A., Borgoltz, A., Roy, C. J., Devenport, W. J. & Lowe, K. T. 2023 Boundary layer flow over a bump and the three-dimensional law of the wall. *Journal of Turbulence* **24** (3-4), 2202404.

Gargiulo, A., Beardsley, C., Vishwanathan, V., Fritsch, D. J., Duetsch-Patel, J. E., Szoke, M., Borgoltz, A., Devenport, W. J., Roy, C. J. & Lowe, K. T. 2020 Examination of flow sensitivities in turbulence model validation experiments. In *AIAA SciTech 2020 Forum*, p. 1583.

Gargiulo, A., Duetsch-Patel, J. E., Borgoltz, A., Devenport, W. J., Roy, C. J. & Lowe, K. T. 2023 Strategies for computational fluid dynamics validation experiments. *Journal of Verification, Validation and Uncertainty Quantification* **8** (3), 031004.

Gargiulo, A., Duetsch-Patel, J. E., Ozoroski, T. A., Beardsley, C., Vishwanathan, V., Fritsch, D., Borgoltz, A., Devenport, W. J., Roy, C. J. & Lowe, K. T. 2021 Flow field features of the BeVERLI Hill model. In *AIAA Scitech 2021 Forum*, p. 1741.

Gray, P., Corke, T., Thomas, F., Gluzman, I. & Straccia, J. 2023 Turbulence model validation through joint experimental/ computational studies of separated flow over a three-dimensional tapered bump. *NASA* .

Haller, G. 2004 Exact theory of unsteady separation for two-dimensional flows. *Journal of Fluid Mechanics* **512**, 257–311.

Narasimha, R. & Sreenivasan, K. 1973 Relaminarization in highly accelerated turbulent boundary layers. *Journal of Fluid Mechanics* **61** (3), 417–447.

Narayanan, M. B. & Ramjee, V. 1969 On the criteria for reverse transition in a two-dimensional boundary layer flow. *Journal of Fluid Mechanics* **35** (2), 225–241.

Serra, M., Crouzat, S., Simon, G., Vétel, J. & Haller, G. 2020 Material spike formation in highly unsteady separated flows. *Journal of Fluid Mechanics* **883**, A30.

Serra, M., Vétel, J. & Haller, G. 2018 Exact theory of material spike formation in flow separation. *Journal of Fluid Mechanics* **845**, 51–92.

Uzun, A. & Malik, M. R. 2021 Simulation of a turbulent flow subjected to favorable and adverse pressure gradients. *Theoretical and Computational Fluid Dynamics* **35**, 293–329.

Vinuesa, R., Bobke, A., Örlü, R. & Schlatter, P. 2016 On determining characteristic length scales in pressure-gradient turbulent boundary layers. *Physics of fluids* **28** (5).

Williams, O. J., Annamalai, H., Ozoroski, T. A., Roy, C. J. & Lowe, K. T. 2022 Comparison of hill-type geometries for the validation and advancement of turbulence models. In *AIAA SCITECH 2022 Forum*, p. 1032.